actuators

MDPI

Article

Experimental Investigation on Flow Control over a Circular Cylinder Using Antiphase Pulsed Jets

Jiaxin Pan, Wanbo Wang *, Xunnian Wang, Chaoqun Li, Xinhai Zhao and Kun Tang

State Key Laboratory of Aerodynamics, China Aerodynamics Research and Development Center, Mianyang 621000, China; bc22005009@mail.ustc.edu.cn (J.P.)
* Correspondence: bowanw@163.com; Tel.: +86-182-2708-8336

Abstract: To investigate the flow control characteristics of antiphase pulsed jet technology and explore a more efficient method to control unsteady flow with minimal impact on flow turbulence, wind tunnel experiments were conducted. The aim was to address the issue of flow separation control on the surface of a cylindrical model. The model had a diameter of 100 mm, and an experimental setup utilizing an antiphase pulsed jet excitation was developed. The optimisation of unsteady jet control involved adjusting parameters such as jet momentum coefficient, slot position, and excitation frequency. The flow separation control effect on the cylinder surface was compared between in-phase and antiphase pulsed jet using a particle image velocimetry (PIV) technique. The mechanisms of flow control for these two methods were analysed. The results showed that in still air, increasing the jet momentum led to a gradual decrease in the high-velocity region, which also moved away from the wall. Under incoming flow conditions, positioning the slot closer to the separation point resulted in better flow separation control, particularly when the excitation frequency matched the main flow frequency. Both in-phase and antiphase pulsed jet excitations effectively suppressed flow separation. In the near-wall region within the symmetric plane between the two slots, the antiphase excitation reduced the root mean square of velocity fluctuations by approximately 1.9% and increased the average velocity by approximately 15.5% compared to in-phase pulsed jet excitation. In-phase pulsed jets exhibited low-frequency, high-velocity characteristics near the separation point, while antiphase pulsed jets, due to the alternating discharge of the two jets, had a lesser impact on the flow field turbulence.

Keywords: wind tunnel test; flow control; PIV measurement; pulsed jet; antiphase

Citation: Pan, J.; Wang, W.; Wang, X.; Li, C.; Zhao, X.; Tang, K. Experimental Investigation on Flow Control over a Circular Cylinder Using Antiphase Pulsed Jets. *Actuators* **2023**, *12*, 432. https://doi.org/10.3390/act12120432

Academic Editor: Luigi de Luca

Received: 17 October 2023
Revised: 16 November 2023
Accepted: 18 November 2023
Published: 21 November 2023

1. Introduction

Flow-around-a-cylinder problems are a classic topic in fluid dynamics. Unsteady flows passing through a blunt body can exhibit large-scale vortex structures, such as the "Kármán Vortex Street", which triggers "Vortex-Induced Vibration (VIV)" [1]. This problem is widely studied in engineering fields, such as vibration, damping, and noise reduction in buildings, including bridges [2,3]. To address these problems, researchers have proposed many passive and active flow control methods, with jet flow control technology in active flow control receiving extensive attention in recent years due to its strong engineering application prospects [4]. Unsteady jets have demonstrated a greater control efficiency than steady jets, with pulsed jet technology being particularly effective [5].

Kong [6] used the large-eddy simulation (LES) method to study how the pulsing frequency affected the mixing efficiency and coherent structures of two jets at different frequencies. Chiatto [7] conducted a study using a spectral proper orthogonal decomposition (SPOD) of pressure measurements and a Fourier analysis of velocity measurements to explore the characteristics of separated flow behind a backward-facing ramp under uncontrolled and pulse-jet-controlled conditions. Pulsed jets are an effective way to alter flow separation by periodically injecting momentum into the flow field, thus improving the

boundary layer's ability to resist reverse pressure gradients. The above view can also be confirmed by the results of Wygnanski [8], Seifert [9], Greenblatt [10], and McManus [11], who used pulsed jets to restrain the flow separation on the airfoil.

For the flow around a cylinder, the critical Reynolds number's magnitude is usually 10^5 [12]. At subcritical Reynolds numbers, the flow through the cylinder is laminar, and the separation location is usually on the windward side of the cylinder [12]. Many research results have been on laminar flow separation on cylindrical surfaces using unsteady jets. Bera et al. [13] used acoustic excitation jet control to effectively inhibit the separation of the airflow on the surface of the cylinder and analysed the induced flow field; Wang et al. [14] applied synthetic jets to the front and rear stationary points of the cylinder to effectively reduce the extent of the separation region of the cylinder; Jukes [15] et al. arranged a DBD plasma near the separation point of the cylinder, and then the separation area of the cylinder was reduced. Jukes et al. [15] arranged DBD plasma excitation pulsed jets near the cylindrical separation point, which could effectively suppress vortex shedding when the dimensionless excitation frequency was three times that of the mainstream frequency, and such airless control methods also include the studies by Jardin [16], Tensi [17], and Fujisawa et al. [18]. All these results show that these excitations have a high control efficiency but are usually limited in terms of momentum input and excitation duration.

The open literature shows fewer studies on active unsteady jet flow separation for cylindrical windings. Zhou et al. [19] investigated the control effect and mechanism of oscillating jets on cylindrical vortex shedding by wind tunnel tests. Two rows of oscillating jet excitations were placed in the cylinders close to the separation point, and the results showed that when the momentum coefficient was 0.2147, compared with the uncontrolled case, the swept jet control reduced the turbulent kinetic energy by 73% and the dimensionless Reynolds shear stress by 68% compared to the natural case. Although the work above achieved a good separation control efficiency, it needed to consider the influence of the phase difference between the jets with different spanwise locations on separation control.

The antiphase pulse excitation was first proposed by Hoell et al. [20] in 2011 for a three-segment wing with a 30° back-sweep angle and other chord-length wing segments. A DES numerical simulation method was applied to compare the two excitation modes based on the synthetic jet (with the presence of the suction process) and the pulsed jet (without the presence of the suction process). The result showed that both excitation modes could effectively reduce the lifting force fluctuations when the phase difference between the two slots was 180°. It is worth noting that the average lift value obtained from the antiphase pulse jet was higher than the in-phase pulse jet. Although this highly efficient unsteady jet control method, which has a smaller impact on the flow field, has been verified using high-precision numerical calculation methods, the simulation results cannot completely replicate the real flow state. Therefore, an experimental verification of this novel excitation method is urgently needed, but there is currently no experimental research on antiphase pulsed excitation. The reason may be that this method requires a precise control of not only frequency and duty cycle but also phase transformation between two jets. This implies that electromagnetic valve-type exciters need to be accompanied by devices capable of adjusting the signal output, adding to the difficulty of the experiment.

This paper investigates the flow control characteristics of a novel antiphase pulsed jet technology through wind tunnel tests. This method can reduce the fluctuation effects caused by the interaction of two jets at the shear layer while maintaining the suppression of flow separation. Addressing the flow control problem in the wake flow around a cylinder, electromagnetic valves are controlled using microcontroller technology to achieve the antiphase pulsed jet excitation. In the wind tunnel tests, the parameters of jet momentum coefficient, slot position, and excitation frequency are varied to optimise the unsteady jet control. The PIV technique is employed to compare the flow separation control effects between in-phase and antiphase pulsed jet excitation, and the flow control mechanism is analysed.

2. Test Equipment and Method

2.1. Wind Tunnel

The experiment was conducted in the Electro-Aerodynamics Research Low-Speed Wind Tunnel of the China Aerodynamic Research and Development Centre (CARDC). The wind tunnel is a direct-current, open-ended wind tunnel with the following dimensions: 0.75 m × 0.75 m × 1.05 m. The stable wind speed ranges from 2 m/s to 55 m/s, with less than 0.2% turbulence. The experimental wind speed was 3 m/s, and the Reynolds number Re ≈ 2×10^4 based on the cylindrical diameter. Reference [21] suggests that at lower Reynolds numbers, the separated shear layer is less affected by the shedding of the Kármán vortex street. The shedding of the Kármán vortex street occurs further downstream. Therefore, choosing a relatively low Reynolds number is appropriate.

2.2. Model and Support

A cylindrical experimental model with a diameter of D = 0.1 m and a spread length of b = 0.48 m was made of hard resin, with two independent rectangular jet slots and ventilation ducts embedded in the cylinder, which could realise the antiphase pulsed jet separation control with two slots blowing alternately, as shown in Figure 1.

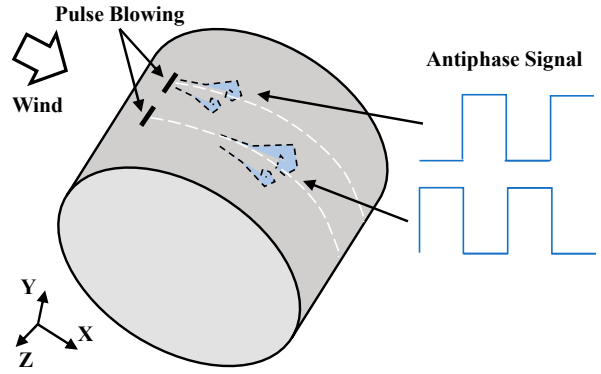

Figure 1. Schematic of antiphase pulse blowing separation control.

The slot size was 1.5 mm (height) × 6 mm (width). The ratio of slots width to the spreading interval was 85%, selected as a smaller reference range in the literature [22] due to the more extensive range of jet diffusion along the spreading direction caused by the slot design. The arrangement of the experimental setup shows in Figure 2. The cylinder was supported vertically and connected to the bottom motor through a support sting. Motor rotation allowed for the adjustment of the slot position. The base of the cylindrical installation was marked with different scale angles. The slot position could be achieved by rotating the model along the scale. Using the upper and lower Plexiglass end plates eliminated the three-dimensional effect and was convenient for carrying out the flow field display and PIV experiments.

2.3. Particle Image Velocimetry Technology

PIV is a nonintrusive experimental technique that tracks particles' motion in a fluid to obtain information about the flow field velocity distribution and turbulent characteristics. When carrying out PIV experiments, the laser sheet was parallel to the cylindrical chordal and spanwise directions. In the chordal direction, it was located in the position of two different slots (Z/b = 44%, Z/b = 54%) and the middle of the two slots in the partition position (Z/b = 50%), see Figure 3a; in the spanwise direction, it was located in the span cross section of the distance downstream from the slot at the distance of X/D = 20%, which was perpendicular to the direction of incoming flow, see Figure 3b. Fluorescent particles were generated by heating the aerosol (DEHS) through the smoke generator with a particle size of about 0.3 μm and the high-speed CCD camera with a resolution of 2048 pixels × 2048 pixels. The cameras were arranged at the top of the wind tunnel and

downstream of the wind tunnel, and the camera axes were vertically intersected with the slice of light in the measurement plane.

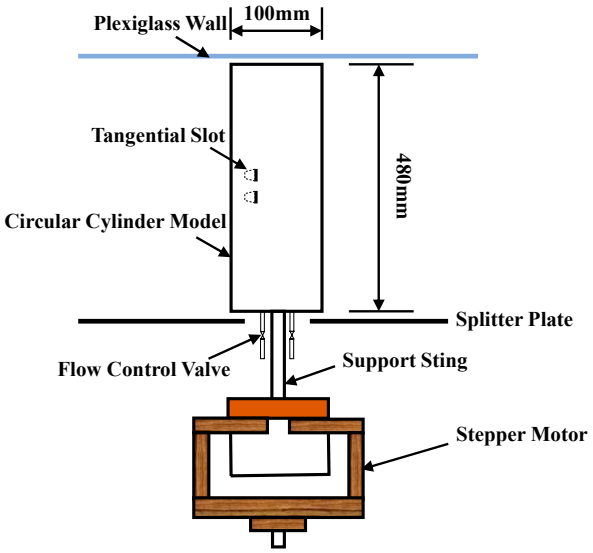

Figure 2. Schematic of experiment setup.

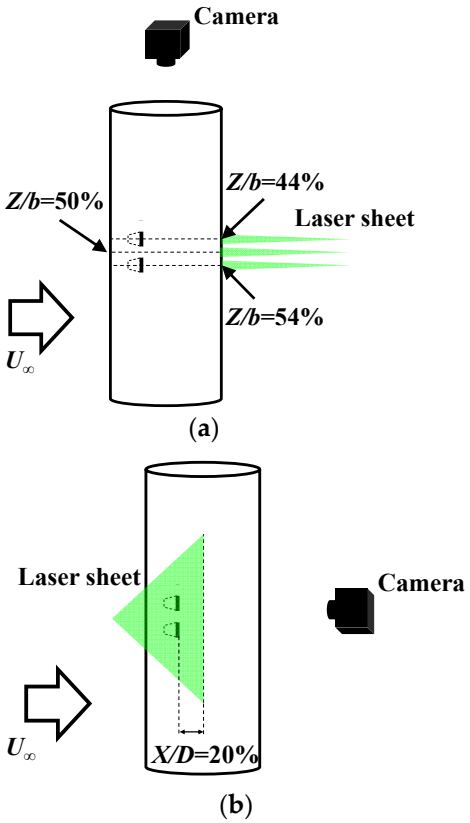

Figure 3. Position diagram of camera and laser: (**a**) chordal direction; (**b**) spanwise direction.

2.4. Actuator and Air Supply System

The unsteady jet from each individual slot was controlled by high-precision electromagnetic valves, specifically the FESTO model MHJ9-QS-6-HF. Before being fed into the model supply pipeline, the compressed air passed through equipment such as an air filter, proportional valve, flow meter, and electromagnetic valve. Compressed air was filtered using an air filter with a mesh size of 5 μm. Flow rate was precisely controlled using a

proportional valve from the SMC brand, with the model number ITV3050-042L. Flow rate was accurately measured using an OMEGA brand flow meter, model FMA-1613-A-B, with a measurement accuracy of approximately 0.001 g/s. The power supply was provided by a high-precision DC stabilized power supply from the UNI-T brand, with the model number UTP1310.

2.5. Signal Output and Acquisition System

The main control chip was a microcontroller with a primary frequency of 72 MHz connected to the proportional valve and solenoid valve output control signals to achieve unsteady jet frequency, duty cycle, the phase difference of the precise control, and acquisition of the flowmeter output data; see Figure 4 for the microcontroller internal structure of the main components.

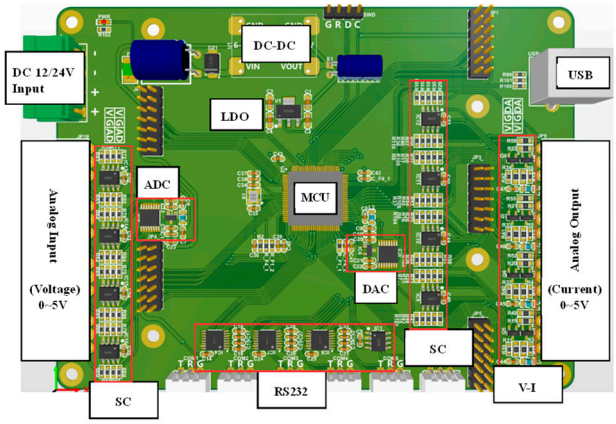

Figure 4. Internal composition of the main control board.

2.6. Hot-Wire Anemometer

To measure velocity fluctuations near the wall between slots and the actual phase difference between the two jets, a Hanghua CTA-04 hot-wire anemometer was used to measure the velocity at the monitoring point. The system consists of two independent working channels, allowing for the simultaneous use of either two single-wire hot-wire probes or one dual-wire probe. During the measurement, the sampling time was set to 0.1 s, and the sampling frequency was 10 kHz. This measurement method has the advantages of a high-frequency response, high accuracy, low temperature drift.

3. Characteristic Study of Jet in Still Air

3.1. Experimental System

To analyse the flow field characteristics of the jet under different momentum, exclude the influence of the incoming flow and slot position, and select a more suitable momentum coefficient for the subsequent jet control separation test, the PIV flow field measurement was carried out under different momentum coefficients in still air (no incoming flow). The same PIV equipment measured the characteristics of the jet-induced flow field under still air and incoming flow conditions.

The cylindrical model with embedded jet slots was placed in a confined space to avoid the interference of ambient airflow on the experimental results, see Figure 5. The experimental method for measuring the exciter in an enclosed space, as described in reference [23], involves using a closed space with dimensions more than 10 times larger than the model diameter to effectively ignore the sidewall influence on the flow field. The laser sheet was located in the chordal direction on the cross section passing through the slot. The DEHS was coated on the conductive cable and placed outside the laser sheet, the conductive cable was heated by electricity to vaporize the DEHS, and the jet could induce the vaporized fluorescent particles into the laser sheet. The PIV system could measure the jet flow field in still air.

The cylinder was mounted vertically in a confined space by a support sting, and the laser sheet was directed parallel to the chordal direction and illuminated the centre of the slot at the Z/b = 44% position. The maximum repetition frequency of the laser was 20 kHz, and the single pulse energy was 30 mj. A CCD camera was arranged above the cylinder, with a resolution of 1024 pixels × 768 pixels, a field of view area of 267 mm × 200 mm, and an acquisition frequency of 4 kHz. The data were processed with an arithmetic window size of 32 pixels × 32 pixels, an overlap rate of 50%, and a velocity error of less than 3%.

Before the experiment, the PIV calibration was performed by a calibration board, controlling the proportional valve and collecting high-intensity flowmeter data to realise tangential jets with different momentum coefficients (calculated from the wind speed under incoming flow conditions). The following equation was used to calculate the dimensionless momentum coefficient:

$$C_\mu = \frac{m_j U_j}{qS} = \frac{m_j}{qS}\left\{\frac{2\gamma RT_0}{\gamma - 1}\left[1 - \left(\frac{P_a}{P_0}\right)^{\frac{\gamma-1}{\gamma}}\right]\right\}^{\frac{1}{2}} \quad (1)$$

where the mass flow rate m_j was measured by a high-precision flow meter, q is the test tachopressure under incoming flow conditions, S is the windward area of the cylinder, and given the pressure ratio, C_μ can be derived. After the jet stabilized, the conductive cable was heated, and the CCD camera started to take pictures.

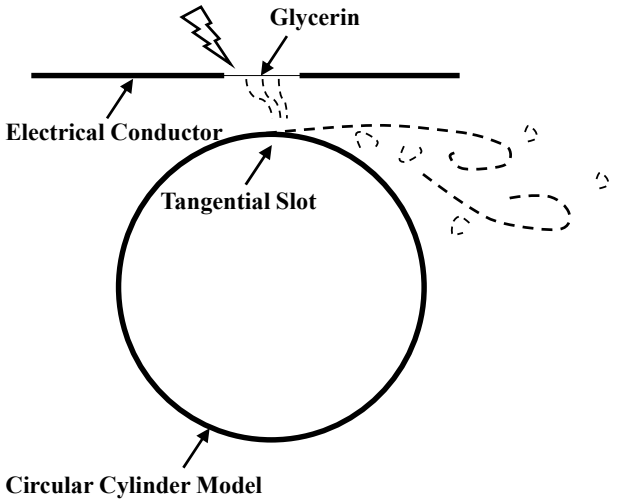

Figure 5. Schematic of actuator characteristic test in still air.

3.2. Experimental Result

The velocity distribution of the jet with different momentum coefficients on the polyline (PL) parallel to the plane of the slot at X/D = 20% downstream is shown in Figure 6, where U/U_∞ is the dimensionless jet velocity, U_∞ is the test wind speed (U_∞ = 3 m/s); h/D is the dimensionless distance, h is the height from the cylinder, and D is the diameter of the cylinder. As shown in Figure 6, the velocity magnitudes of the three different momentum coefficients at the polyline do not differ much due to the small magnitude of the test wind speed. With the increase in momentum, the maximum jet velocity increases sequentially by about 4%, and the region with a higher velocity gradually shrinks and moves along the direction away from the wall.

Considering that the higher velocity region of the jet with C_μ = 0.005 is closer to the cylindrical wall and the Coanda effect is more prominent, we selected that C_μ for the subsequent experiments under the incoming flow condition.

The actual phase difference between the two jets was measured using the hot wire in still air, as shown in Figure 7. The excitation frequencies were set at 24 Hz, 48 Hz, and 72 Hz, corresponding to dimensionless frequencies of 0.8, 1.6, and 2.4, respectively, with

a duty cycle of 50%. It can be observed that at different excitation frequencies, the two nozzles exhibit alternating blowing phenomena, and the actual phase difference remains around 180°. This indicates that the microcontroller technology employed in this study can achieve a phase adjustment in antiphase.

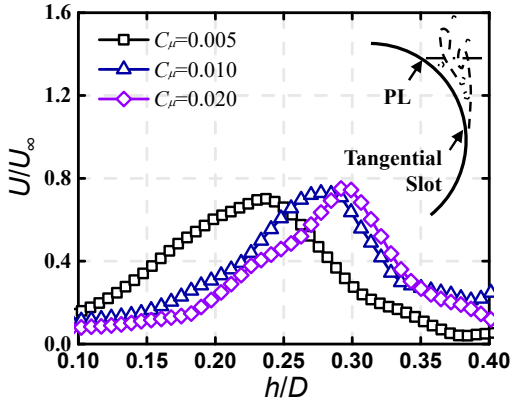

Figure 6. Velocity distribution of jets with different momentum coefficients in still air.

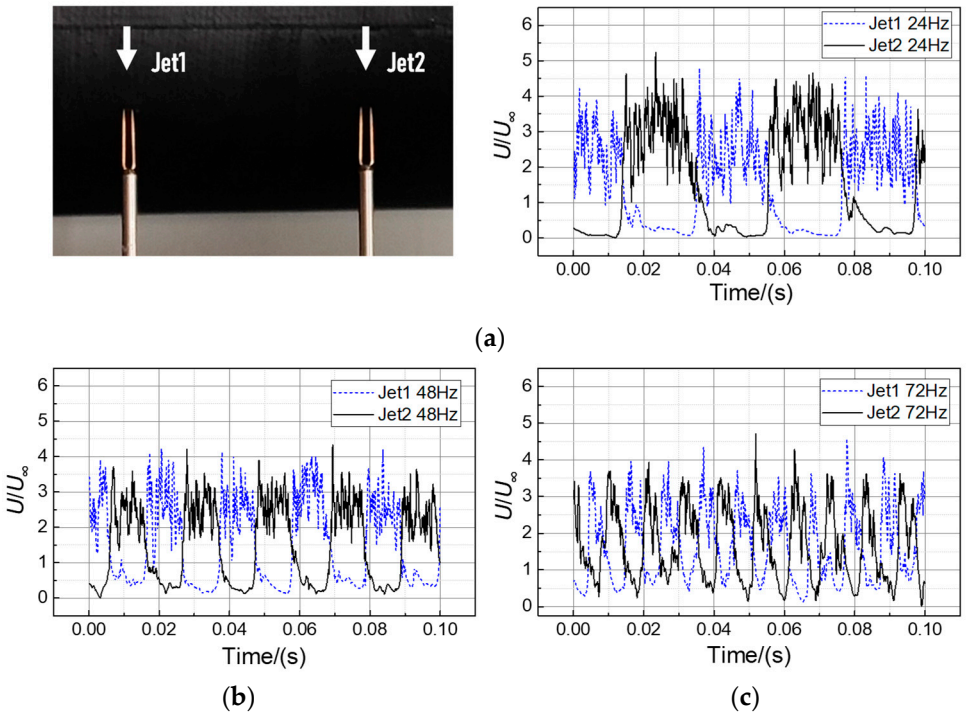

Figure 7. The actual phase difference between the two jets of different excitation frequencies: (**a**) *St* = 0.8; (**b**) *St* = 1.6; (**c**) *St* = 2.4.

4. Results of Flow Separation Control

4.1. Different Slot Positions

Under the incoming flow conditions, the first investigation was tangential constant jet flow field characteristics at different slot positions.

According to the location of the separation point of the cylinder under different Reynolds numbers summarized in the literature [24], the separation point under the test Reynolds number in this paper was near the position of 80°~85°, so the influence of the slot position on the separation control was studied at four places before and after the separation point, which were 60°, 75°, 90°, and 105°, respectively.

From Figure 8a–d, the characteristics of the flow field are basically the same—the separation points from the streamlines are all near 80°. The position of the shear layer and

the range of the separation region are also not much different, which indicates that the influence of the repair pattern near the tangential slot on the flow field can be ignored.

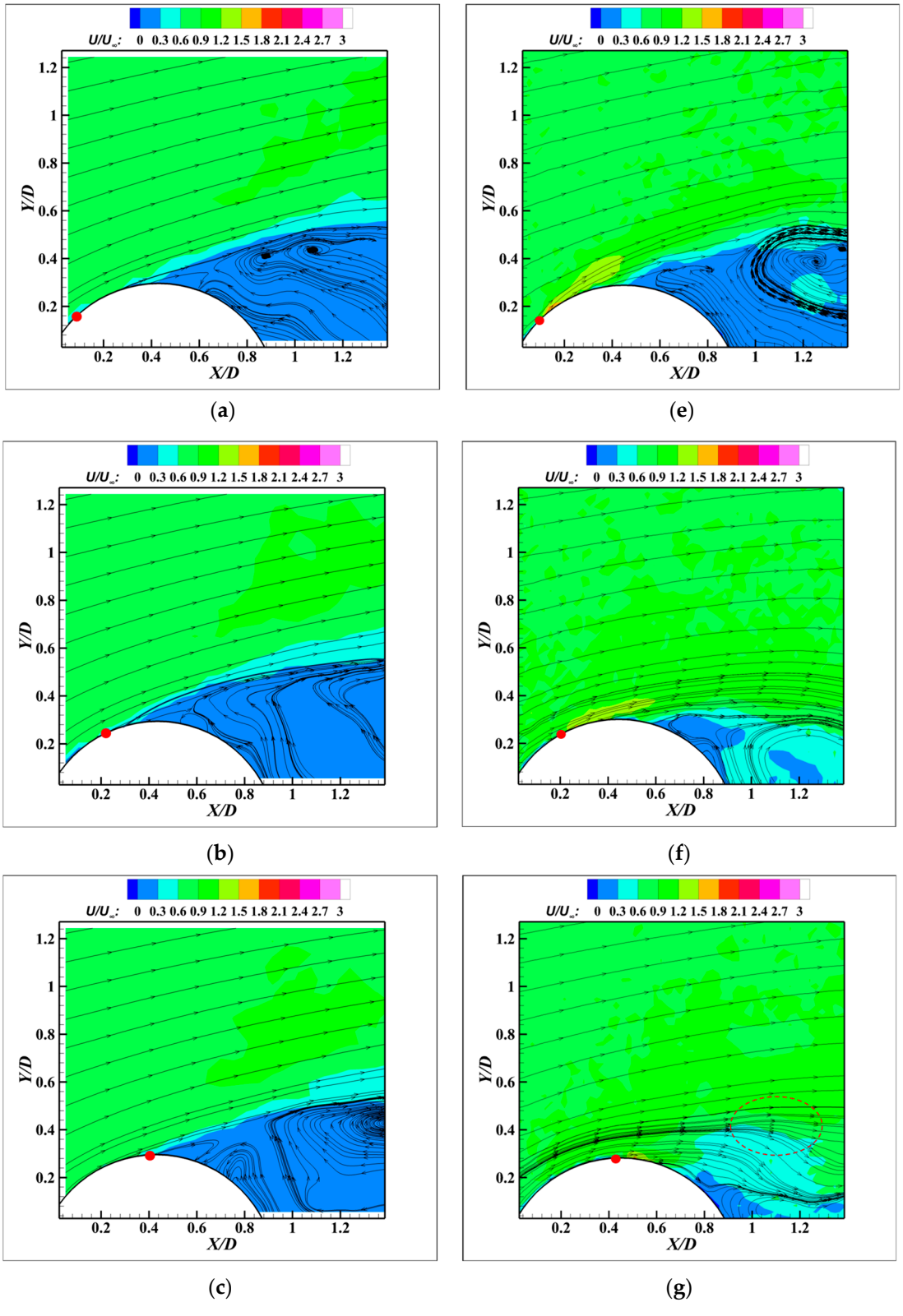

Figure 8. *Cont.*

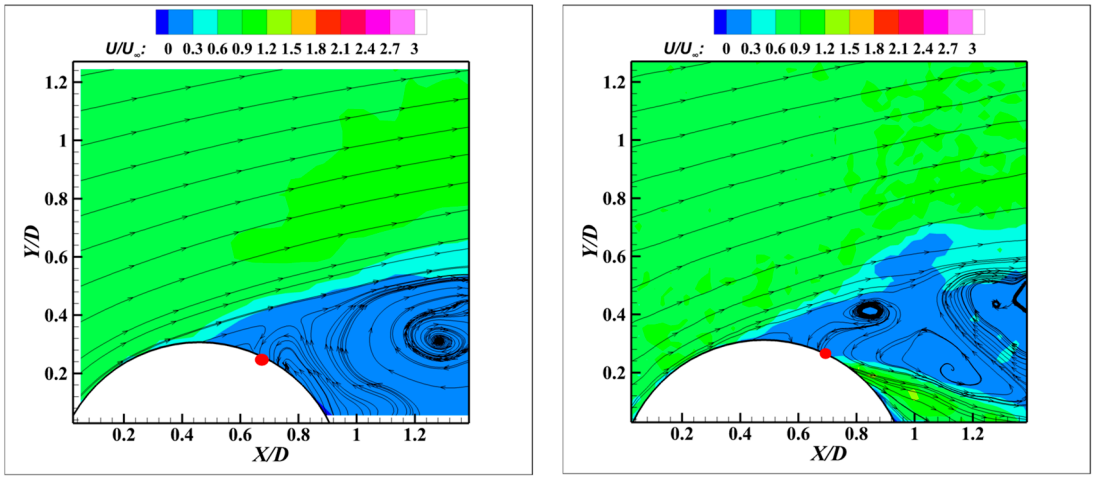

(**d**) (**h**)

Figure 8. The time-averaged results of different slot positions' separation control(the red dots indicate the jet positions): (**a**) natural case at 60°; (**b**) natural case at 75°; (**c**) natural case at 90°; (**d**) natural case at 105°; (**e**) applied blowing control at 60°; (**f**) applied blowing control at 75°; (**g**) applied blowing control at 90°; (**h**) applied blowing control at 105°.

From Figure 8e–h, the separation control effect is better when the slot position is at 75° and 90°. Compared with the results of the flow field at 60° and 105°, the jet excitation is closer to the separation point at 75° and 90°, which has a more substantial effect on the separation of the shear layer. Comparing the results in Figure 8f,g, the jet is less affected by the wall friction at 90° and the jet along the slot in the normal direction, and with the gradual increase in the jet spreading range, the flow line bends at 0.4 D from the slot, as marked by the red dashed line in Figure 8g. In comparison, the flow line at 75° is smoother and gradually transitions to the direction of the separation region. Considering the cost of the test and the research focus, this test did not continue to optimise the slot position more finely, so the subsequent test at the 75° slot position to study the effect of the unsteady jet on the separation control of the cylindrical flow.

4.2. Different Excitation Frequency

Frequency and duty cycle are two fundamental parameters in the control of nonconstant jets. This paper mainly studied jet control based on two slots. Hence, the duty cycle was not a key parameter to study and was set to 50%, to study the separation control under different jet frequencies. The dimensionless shedding frequency (Strouhal number) is defined in Equation (2):

$$St = \frac{Df}{U_\infty} \tag{2}$$

where D is the diameter of the cylinder, and f is the frequency. The Q-criterion vortex identification method in reference [25] with no control applied is shown in Equation (3):

$$Q = -\frac{1}{2}\left[\left(\frac{\partial u}{\partial x}\right)^2 + \left(\frac{\partial v}{\partial y}\right)^2\right] - \frac{\partial u}{\partial y}\frac{\partial v}{\partial x} \tag{3}$$

where u and v are the velocities in the x and y directions, respectively; as shown in Figure 9, the vortex pairs with different rotational directions were alternately distributed near the shear layer. Observing the results of the Q-criterion isosurfaces at different moments, the vortex shedding frequency (St) near the cylindrical separation point was about 1.6. Therefore, the excitation frequencies were set to be 0.8, 1.6, and 2.4, and the momentum coefficients of the pulsed jet, $C_{\mu,eff} = DC \times C_\mu$, were as defined in the literature [26], which were obtained as $C_{\mu,eff} = 0.025$ by the product of the duty ratio and the steady jet momentum coefficient. At this pulsed jet momentum coefficient, Figure 10 gives the experimental

results of the dimensionless velocity contours of the flow field. From the results, when the excitation's nondimensional frequency was 1.6, the range of the low-velocity separation region ($U/U_\infty \leq 0.3$) was similar to that found in the literature [4]. The control effect is better when the excitation frequency is close to the primary frequency of the incoming flow, so the next test was under the excitation frequency of 1.6 and a duty cycle of 50%.

4.3. Velocity Patterns at Dual Slots and Their Intervals

Before carrying out the dual-slot flow control tests, to determine the effect of the jet flow differences between the different slots on the experimental results, the jet velocity patterns of the two slots were measured separately. The laser sheet was positioned as shown in Figure 3a, and the time-averaged jet velocity pattern on the polyline parallel to the plane of the slots at the distance of X/D = 20% downstream of the slots was determined, as shown in Figure 11. The maximum velocity magnitude and distribution of the two jets were the same. The velocity pattern in the middle of the two slots (Z/b = 50%) showed that the maximum jet velocity was also located near h/c = 0.8 due to the intersection of the two jets. The velocity was gradually close to the incoming velocity (U/U_∞ = 1) as it moved away from the wall.

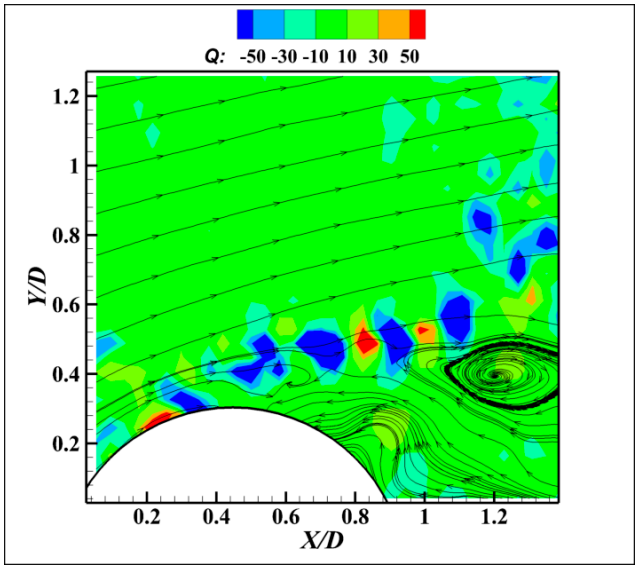

Figure 9. Q criterion isosurface countor in natural case.

4.4. In-Phase and Antiphase Pulsed Jet Excitation

4.4.1. Input Signal Description

When the two slots are in the same phase when opening the pulse jet, the solenoid valves controlling the two jets are opened and closed at the same time, and the signal input to the solenoid valve is shown on the right side of Figure 12a. To operate the two jets, we opened and closed the solenoid valves alternately after shifting the excitation signal of one slot by 180° in phase, and the signal input to the solenoid valve is shown on the right side of Figure 12b. Due to the duty cycle of 50%, from a spatial point of view, the antiphase pulse jet excitation was repeatedly changed between the two slots; from a temporal point of view, considering the two slots as a whole, the jet excitation was kept continuous in time.

4.4.2. Velocity Changes at Different Monitoring Points

Under the in-phase and antiphase pulsed jet excitation, respectively, the dimensionless velocity and the change in velocity direction at the monitoring points near the upstream of the separation point shown in Figure 13 were calculated by the PIV postprocessor. Three monitoring points were located on the Z/b = 50% plane. The distances along the incoming direction of the flow to the slots were all X/D = 20%. Monitoring points 1 to 3 were located

at the distances from the cylindrical wall at h/D = 1%, 11%, and 21%, respectively, from the cylindrical wall.

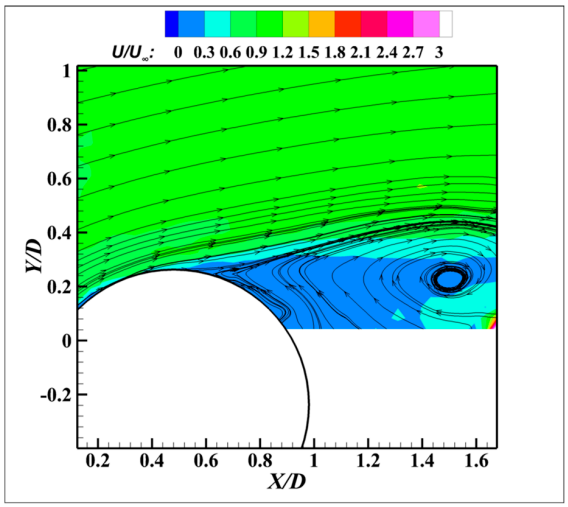

(**a**)

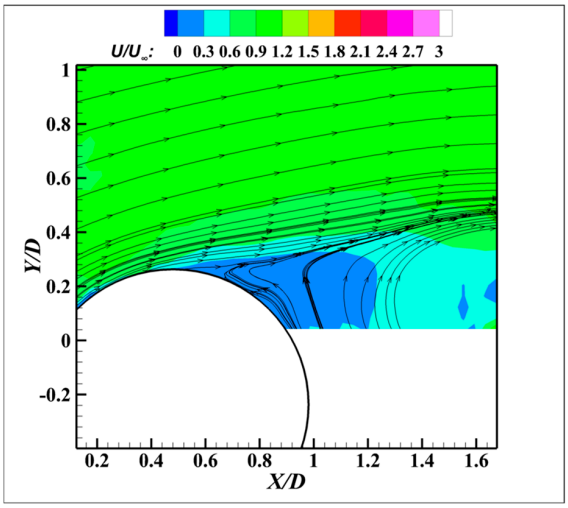

(**b**)

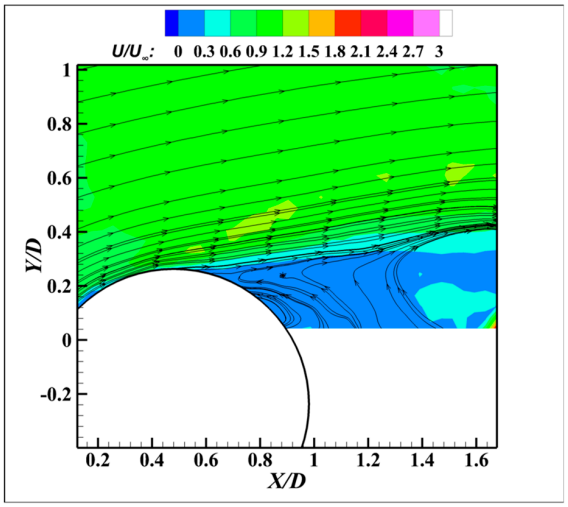

(**c**)

Figure 10. Results of different excitation frequencies: (**a**) St = 0.8; (**b**) St = 1.6; (**c**) St = 2.4.

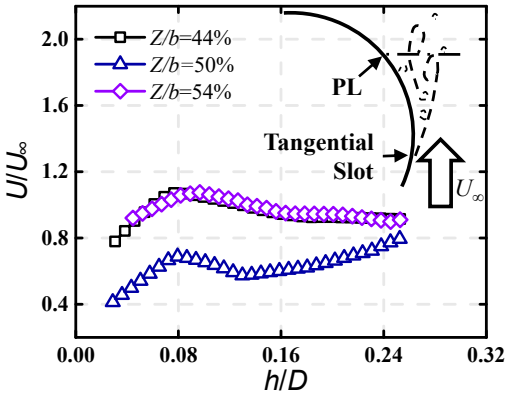

Figure 11. Velocity distribution of two slots and its spacing.

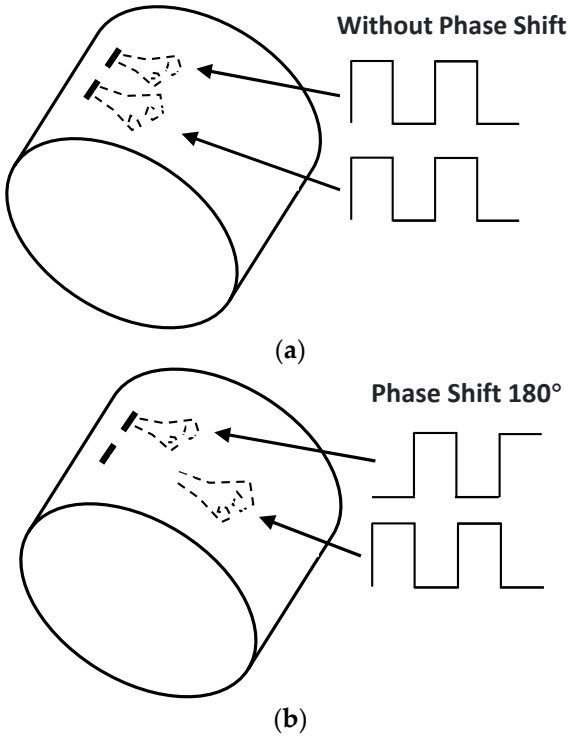

Figure 12. Schematic of pulse jets in the same phase and in antiphase: (**a**) in-phase; (**b**) antiphase.

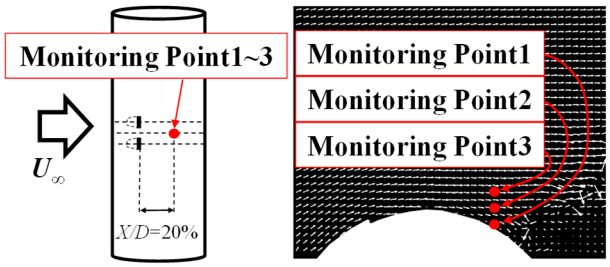

Figure 13. Location of monitoring points.

The velocity within 25 ms after stabilisation of the control is given in Figure 14. Compared with the in-phase, the fluctuation in dimensionless velocities at all three monitoring points was more insignificant with the antiphase. The mean value of the velocity at monitoring point 1 near the wall increased by about 15.5%, as shown in Figure 14a. As the monitoring points moved away from the wall and approached the core of the jet, the mean values of the velocities at the two modes became closer.

Figure 15 shows the RMS velocity at different monitoring points. RMS is the square sum of the deviation of the test value x from the mean value μ and the square root of the ratio of the number of observations N, as follows:

$$\sigma_{SD} = \sqrt{\frac{1}{N}\sum_{i=1}^{N}\left(x^{(i)} - \mu\right)^2} \tag{4}$$

where x is the test result at the monitoring point, and μ is the average value of several test results at the monitoring point. The dimensionless RMS velocity variance at the three monitoring points near the wall after the antiphase pulsed jet excitation was smaller than that of the in-phase pulsed jet excitation. The RMS variance between the in-phase and antiphase velocity at monitoring points 1 to 3 were 1.9%, 4.5%, and 6.7%, respectively. The fluctuations of the flow field were more and more violent with the in-phase than the antiphase as the monitoring points were far away from the wall and closer to the core of the jet.

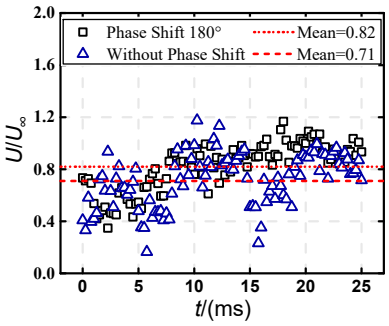

(**a**)

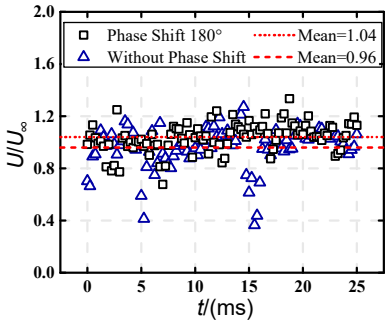

(**b**)

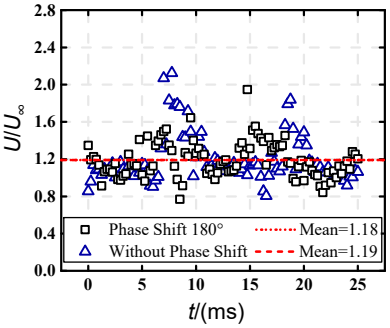

(**c**)

Figure 14. Dimensionless velocity at different monitoring points: (**a**) monitoring point 1; (**b**) monitoring point 2; (**c**) monitoring point 3.

The velocity direction fluctuated above and below θ_{jet} = 170° for both in-phase and antiphase excitations, which was close to the local tangential angle, indicating that both modes effectively restrained the flow separation, see Figure 16. The amplitude of the fluctuation in the velocity direction vector was also smaller after the antiphase excitation. The velocity at monitoring point 1 was measured using the Hanghua CTA04 hot-wire anemometer. The obtained power spectral densities (PSDs) are shown in Figure 17. The PSD was calculated following the method described in reference [27]. To ensure data authenticity, the data were not filtered. The results indicated that there was a peak (the red dotted circle) at the excitation frequency of 48 Hz (St = 1.6) in the PSD without a phase shift. However, after a phase shift of 180°, the peak disappeared, reducing the velocity fluctuation.

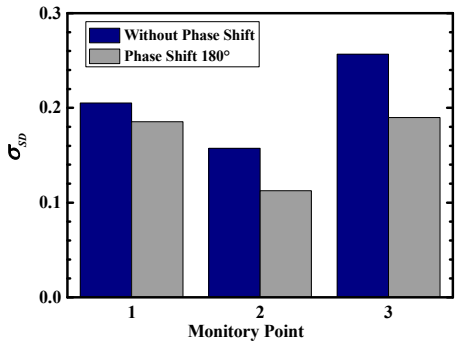

Figure 15. Dimensionless RMS velocity at different monitory points.

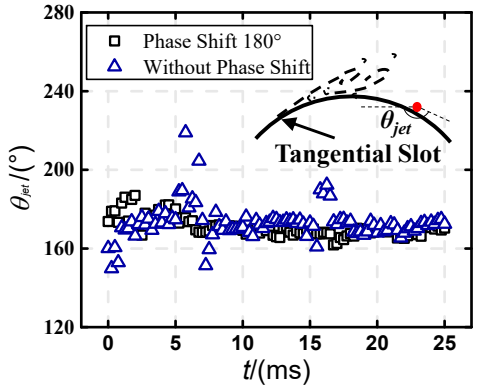

Figure 16. Velocity direction change under excitation with in-phase and antiphase pulses (St = 1.6, $C_{\mu,eff}$ = 0.025).

In summary, both in-phase and antiphase pulse jet excitations could effectively restrain flow separation. Compared with the in-phase pulse jet excitation in the middle of the two slots near the wall at the partition location, the magnitude of the velocity fluctuation was weaker, and the average value of the velocity was more significant after the antiphase excitation.

4.4.3. Chordal Cross Section's Velocity Field at the Interruption

In order to analyse the reason for this result, the characteristics of the induced flow field under in-phase and antiphase pulsed jet excitations with were analysed. The instantaneous induced velocity field at the Z/b = 50% cross section is given in Figures 18 and 19, respectively. The white arrows represent the local velocity vectors, and the longer arrows represent the higher velocity, where the results in Figures 18 and 19a–f correspond to the following time intervals from turning on the jet excitation, respectively: 0 ms, 5.0 ms, 10.0 ms, 20.0 ms, 25.0 ms, and 30 ms.

As shown in Figure 18, the cycle change from the first to the second jet was completed from 5 ms to 25 ms under the in-phase pulse jet excitation. Moreover, from the results in

Figure 19, two-cycle changes from the first to the third jet were completed from 5 ms to 25 ms under the antiphase pulse jet excitation. The antiphase pulse jet velocity was weaker than the in-phase one, and the effect on the flow field fluctuation was negligible. Combined with Figure 17, the jet development area was farther away from monitoring point 1, and the excitation frequency was not expressed in the spectrum of the velocity direction change.

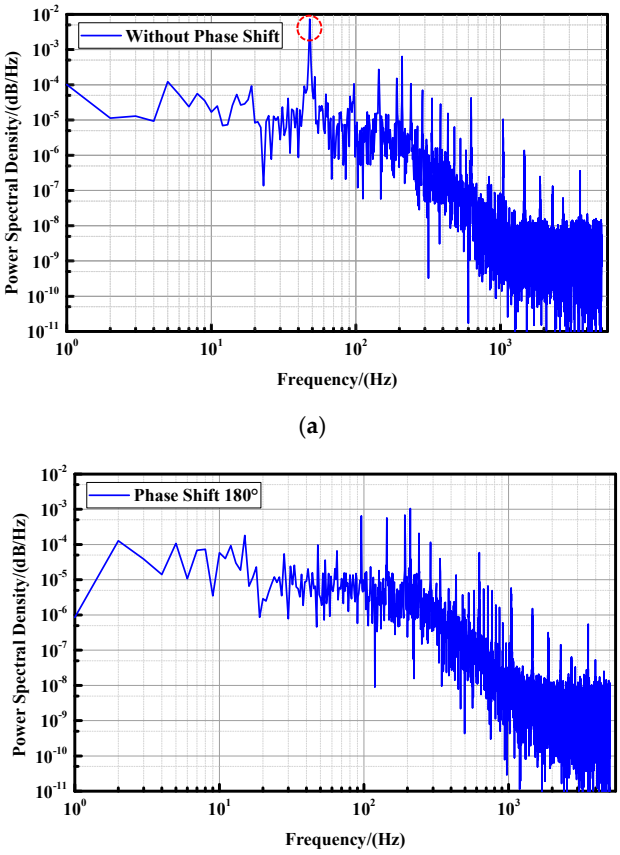

Figure 17. Velocity PSD of monitoring point 1 under excitation with in-phase and antiphase pulses: (**a**) without phase shift; (**b**) phase shift 180°.

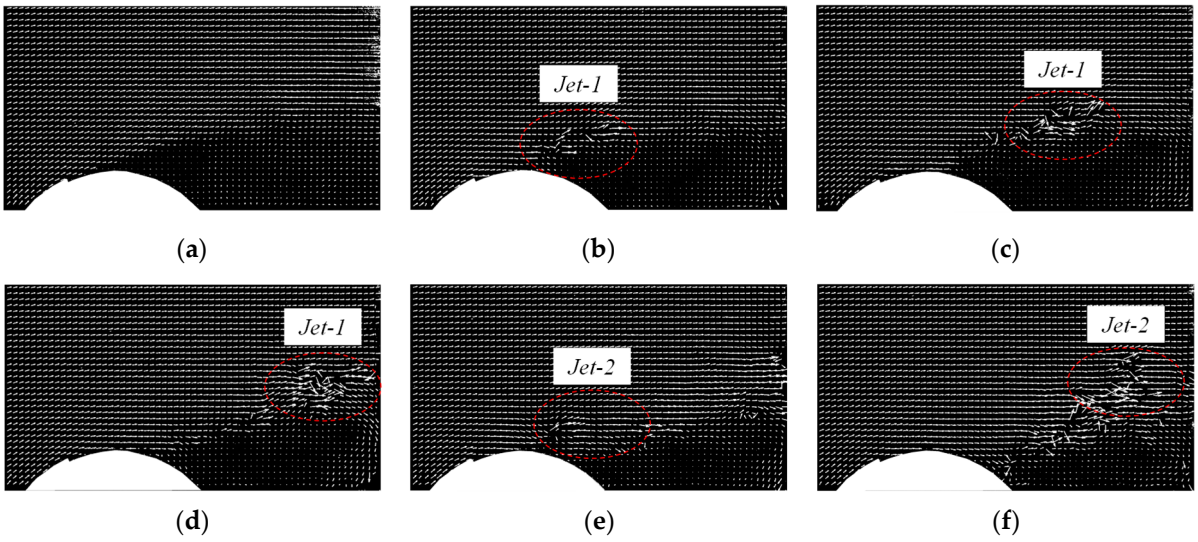

Figure 18. The change in induced velocity field with time under the excitation of an in-phase pulsed jet: (**a**) 0 ms; (**b**) 5.0 ms; (**c**) 10.0 ms; (**d**) 20.0 ms; (**e**) 25.0 ms; (**f**) 30 ms.

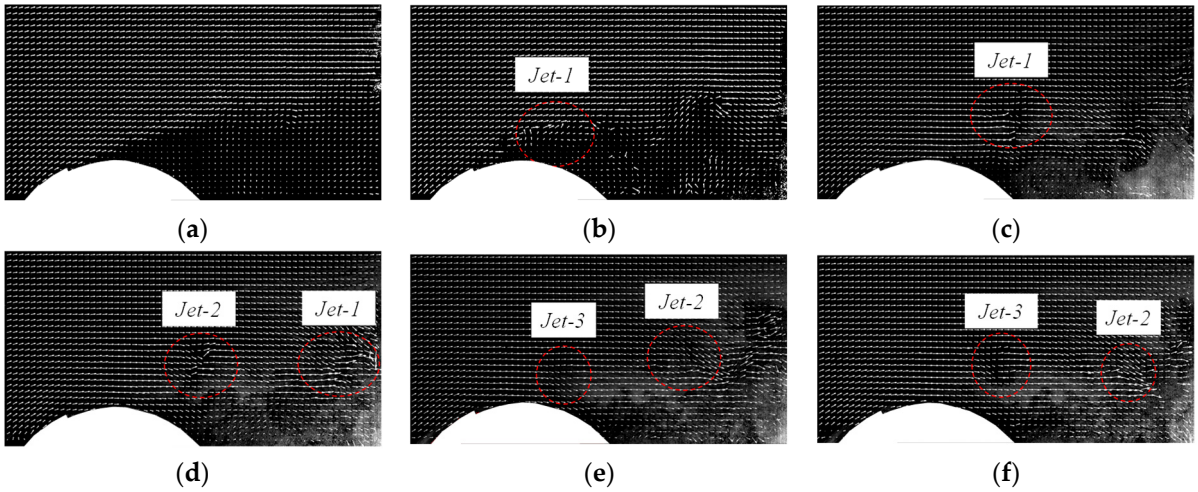

Figure 19. The change in induced velocity field with time under the excitation of a pulsed jet antiphase: (**a**) 0 ms; (**b**) 5.0 ms; (**c**) 10.0 ms; (**d**) 20.0 ms; (**e**) 25.0 ms; (**f**) 30 ms.

4.4.4. Vortices within the Chordwise Cross Section

The instantaneous Q criterion isosurface contour within the Z/b = 50% cross section 30 ms after switching on the jet excitation is given in Figure 20.

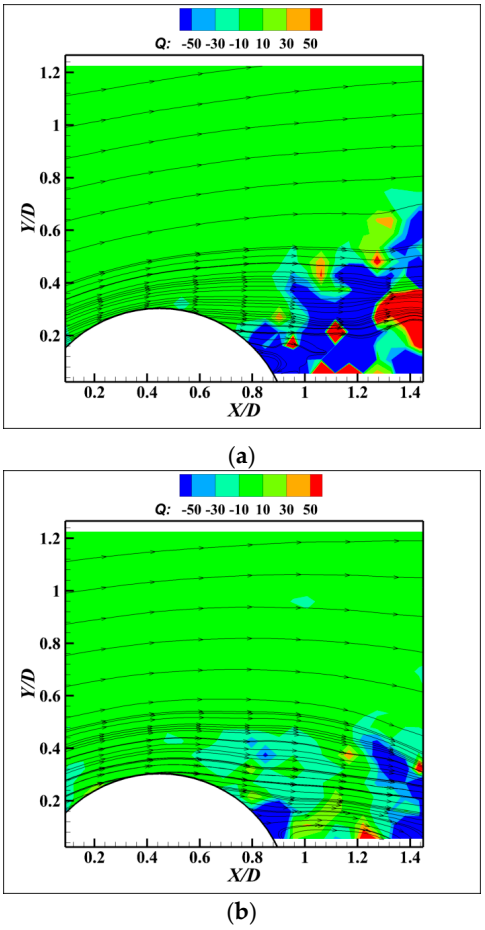

Figure 20. Q criterion isosurface contour under the excitation of in-phase and antiphase pulses: (**a**) in-phase; (**b**) antiphase.

The flow separation control was gradually stabilised 30 ms after the jet excitation was turned on. Combining Figures 18f and 20a, under the in-phase excitation, the whole jet

region gradually spread out and had a higher momentum, which affected the surrounding flow in a broader range and induced multiple vortex structures with larger scales in the cylindrical wake region; combining Figures 19f and 20b, under the antiphase excitation, the jet region dispersed and had a lower momentum, the vortices in the wake region had minor scales, the flow line was smoother than that of the in-phase excitation and transited to the direction of the separation region.

4.4.5. Spanwise Cross Section's Velocity Field

Figure 21 shows the instantaneous velocity along the incoming flow direction to the slot at a distance of X/D = 20%, which was taken 25 ms after excitation, and the way it was shot is shown in Figure 3b. From Figure 21a,b, in the range of the jet region, a more obvious high-speed jet region can be seen, and the magnitude of the velocity was similar, indicating that the main difference between the two ways for the excitation signal phase was different. In Figure 21a, a small high-speed region (marked by the white dashed line) appears, possibly generated by the intersection of the two jets at the separation position (Z/b = 50%), and this phenomenon was also reflected in the results given in Figure 11. However, in Figure 21b, this phenomenon is not seen because the two jets were staggered. It may be the main reason for the difference in velocity fluctuations under in-phase and antiphase excitations.

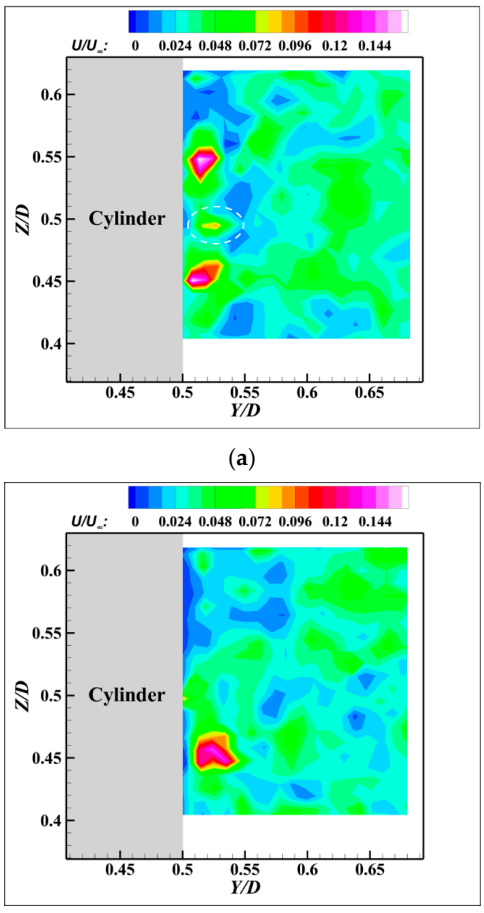

(**a**)

(**b**)

Figure 21. Spanwise velocity contours under the excitation of in-phase and antiphase pulses: (**a**) in-phase; (**b**) antiphase.

4.4.6. Reduction of Frequency and Momentum

To exclude the discrepancy between the in-phase and antiphase pulse excitation results caused by too large a momentum coefficient and too small an excitation frequency, the jet

momentum coefficient was reduced to 0.0125, and the dimensionless excitation frequency was increased to 2.4. Since the separation suppression effect was weakened under this excitation condition, the monitoring point was chosen to be near the shear layer, at a distance of X/D = 5% from the slot. The change in the direction of the velocity at that location is given in Figure 22.

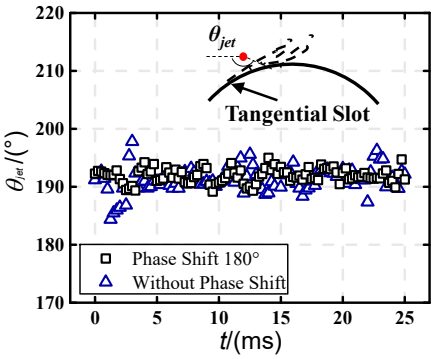

Figure 22. Velocity direction change under the excitation of in-phase and antiphase pulses (St = 1.6, $C_{\mu,eff}$ = 0.0125).

Similar to the results shown in Figure 16, the amplitude of the velocity direction fluctuation was also smaller after shifting the phase, indicating that the different phase between the two modes is the main factor that causes the difference in the velocity fluctuation.

5. Conclusions

This paper conducted wind tunnel tests to validate the advantages of a novel antiphase pulsed jet technology and fill the research gap in experimental aspects of this technology. The following conclusions were obtained:

(1) Using induced fluorescent particles in still air, the velocity distributions of jets with different momentum coefficients at the polyline were measured. It was observed that as the jet momentum increased, the area of higher velocities gradually contracted and moved away from the wall. It was determined that $C\mu$ = 0.005 was an appropriate value.

(2) Under incoming flow conditions, better control effects were achieved when the slot position was closer to the separation point and the excitation frequency was similar to the primary frequency of the flow.

(3) In-phase and antiphase excitations can effectively restrain the flow separation. However, the magnitude of the velocity fluctuation after the antiphase excitation was weaker than that in the in-phase excitation. The mean value of the velocity increased by about 15.5% in the separation position.

(4) The two jets excited by the antiphase pulse jet excitation were staggered, which had less effect on the fluctuation in the flow field.

From a temporal perspective, regarding the two slots as a single entity, the jet excitation was maintained continuously over time. Further research will involve studying additional jet slots and phase changes to enhance control efficiency. Various measurements will be used to analyse the flow mechanism and support the engineering applications of this technology.

Author Contributions: Conceptualization, J.P. and W.W.; methodology, J.P.; software, W.W.; data curation, K.T.; formal analysis, C.L.; writing—original draft preparation, J.P.; writing—review and editing, X.Z.; supervision, X.W. and W.W.; project administration, W.W.; funding acquisition, W.W. All authors have read and agreed to the published version of the manuscript.

Funding: This work was sponsored by the foundation of National Key Laboratory of Science and Technology on Aerodynamic Design and Research (No. 61422010301).

Data Availability Statement: Data are contained within the article.

Conflicts of Interest: The authors declare no conflict of interest.

References

1. Choi, H.; Jeon, W.P.; Kim, J. Control of flow over a bluff body. *Annu. Rev. Fluid Mech.* **2008**, *40*, 113–139. [CrossRef]
2. Wu, Z.; Choi, H. Modification of flow behind a circular cylinder by steady and time-periodic blowing. *Phys. Fluids* **2021**, *33*, 115126. [CrossRef]
3. Yun, J.; Lee, J. Active proportional feedback control of turbulent flow over a circular cylinder with averaged velocity sensor. *Phys. Fluids* **2022**, *34*, 095133. [CrossRef]
4. McLean, J.D.; Crouch, J.D.; Stoner, R.C.; Sakurai, S.; Seidel, G.E. *Study of the Application of Separation Control by Unsteady Excitation to Civil Transport Aircraft: Technical Report CR-1999-209338*; NASA: Washington, DC, USA, 1999.
5. Collis, S.; Ronald, D.; Seifert, A.; Theofilis, V. Issues in active flow control: Theory, control, simulation, and experiment. *Prog. Aerosp. Sci.* **2004**, *40*, 237–289. [CrossRef]
6. Kong, B.; Li, T.; Eri, Q. Large eddy simulation of turbulent jet controlled by two pulsed jets: Effect of forcing frequency. *Aerosp. Sci. Technol.* **2019**, *89*, 356–369. [CrossRef]
7. Chiatto, M.; Hlevca, D.; Grasso, F.; Luca, L.D. Modal analysis of actively controlled flow past a backward facing ramp. In Proceedings of the AIAA SciTech 2020 FORUM, Orlando, FL, USA, 6–10 January 2020.
8. Wygnanski, I. Boundary layer and flow control by periodic addition of momentum. In Proceedings of the 49th AIAA Shear Flow Conference, Snowmass Village, CO, USA, 29 June–2 July 1997; AIAA: Snowmass, CO, USA, 1997; pp. 1–10.
9. Seifert, A.; Bachart, T.; Koss, D.; Shepshelovitch, M.; Wygnanski, I. Oscillatory blowing: A tool to delay boundary-layer separation. *AIAA J.* **1993**, *31*, 2052–2060. [CrossRef]
10. Greenblatt, D.; Darabi, A.; Nishri, B.; Wygnanski, I. Separation control by periodic addition of momentum with particular emphasis on dynamic stall. In *Heli Japan 98*; American Helicopter Society: Gifu, Japan, 1998; pp. T3–T4.
11. McManus, K.R.; Legner, H.H.; Davis, S.J. Pulsed vortex generator jets for active control of flow separation. In Proceedings of the 25th AIAA Fluid Dynamics Conference, Colorado Springs, CO, USA, 20–23 June 1994; AIAA: Colorado Springs, CO, USA, 1994.
12. Kundu, P.K.; Cohen, I.M. *Boundary-Layer Theory*, 9th ed.; Springer: Berlin/Heidelberg, Germany, 2017.
13. Bera, J.C.; Michard, M.; Sunyach, M.; Comte-Bellot, G. Changing lift and drag by jet oscillation: Experiments on a circular cylinder with turbulent separation. *Eur. J. Mech. B-Fluids* **2000**, *19*, 575–595. [CrossRef]
14. Wang, J.J.; Feng, L.H.; Xu, C.J. Experimental investigations on separation control and flow structure around a circular cylinder with synthetic jet. *Sci. China Ser. E Technol. Sci.* **2007**, *50*, 550–559. [CrossRef]
15. Jukes, T.N.; Choi, K.S. Flow control around a circular cylinder using pulsed dielectric barrier discharge surface plasma. *Phys. Fluids* **2009**, *21*, 589. [CrossRef]
16. Jardin, T.; Bury, Y. Lagrangian and spectral analysis of the forced flow past a circular cylinder using pulsed tangential jets. *J. Fluid Mech.* **2012**, *696*, 285–300. [CrossRef]
17. Tensi, J.; Boué, I.; Paillé, F.; Dury, G. Modification of the wake behind a circular cylinder by using synthetic jets. *J. Vis.* **2002**, *5*, 37–44. [CrossRef]
18. Fujisawa, N.; Takeda, G.; Ike, N. Phase-averaged characteristics of flow around a circular cylinder under acoustic excitation control. *J. Fluids Struct.* **2004**, *19*, 159–170. [CrossRef]
19. Zhou, K.; Li, Z.; Liu, Y.; Wen, X. Sweeping jet control of flow around a circular cylinder. *Exp. Therm. Fluid Sci.* **2022**, *141*, 110785. [CrossRef]
20. Hoell, T.; Job, A.K.V.; Giacopinelli, P.; Thiele, F. Detached-Eddy Simulation of Pulsed Blowing Actuation on the Flap of a High-Lift Configuration. In Proceedings of the 29th AIAA Applied Aerodynamics Conference, Honolulu, HI, USA, 27–30 June 2011.
21. Thompson, M.C.; Hourigan, K. The shear-layer instability of a circular cylinder wake. *Phys. Fluids* **2005**, *17*, 021702. [CrossRef]
22. Hoell, T.; Job, A.K.V.; Giacopinelli, P.; Thiele, F. Numerical Study of Active Flow Control on a High-Lift Configuration. *J. Aircr.* **2012**, *49*, 1406–1422. [CrossRef]
23. Zhang, X.; Huang, Y.; Li, H. Flow control over a circular cylinder using plasma actuators. *Chin. J. Theor. Appl. Mech.* **2018**, *50*, 1396–1405.
24. Jiang, H. Separation angle for flow past a circular cylinder in the subcritical regime. *Phys. Fluids* **2020**, *32*, 014106. [CrossRef]
25. Silva, B.; Jose, C. Invariants of the velocity-gradient, rate-of-strain, and rate-of-rotation tensors across the turbulent/nonturbulent interface in jets. *Phys. Fluids* **2008**, *20*, 765. [CrossRef]
26. Cetin, C.; Celik, A.; Yavuz, M.M. Control of Flow Structure over a Nonslender Delta Wing Using Periodic Blowing. *AIAA J.* **2018**, *56*, 90–99. [CrossRef]
27. Feltekh, K.; Jemaa, Z.B.; Fournier-Prunaret, D.; Belghith, S. Border collision bifurcations and power spectral density of chaotic signals generated by one-dimensional discontinuous piecewise linear maps. *Commun. Nonlinear Sci. Numer. Simul.* **2014**, *19*, 2771–2784. [CrossRef]